Nature of lossy Bloch states in polaritonic photonic crystals

Kerwyn Casey Huang,* Elefterios Lidorikis, Xunya Jiang, John D. Joannopoulos, and Keith A. Nelson
Center for Materials Science and Engineering, Massachusetts Institute of Technology, Cambridge, Massachusetts 02139

Peter Bienstman
Department of Information Technology, Ghent University, Belgium

Shanhui Fan
Department of Electrical Engineering, Stanford University, Stanford, California 94305, USA
(Received 25 August 2003; revised manuscript received 2 November 2003; published 27 May 2004)

We examine the effects of absorption losses in photonic crystal structures composed of polar materials which exhibit transverse phonon-polariton excitations. In order to explore the Bloch states of such a system, we study the two subspaces of the complete set of complex (k,ω) states consisting of either real frequency, accessible through a frequency-domain method, or real-wave vector, which we determine using a frequency-dependent time-domain method. We describe analytically the conditions under which the imaginary frequency component of a real-wave-vector state is related to the imaginary-wave-vector component of a real-frequency state through a factor of the group velocity, and we present a one-dimensional lossy crystal as an example that satisfies these constraints. We also discover that the real-frequency states of a two-dimensional crystal bear little resemblance to the class of real-wave-vector states, due to interplay between the prohibitively large spatial decay of the states near the edge of the Brillouin zone and the existence of metalliclike states localized to the surrounding ambient dielectric region with much lower levels of loss. We then put these results in the context of possible experiments, including reflection of a plane-wave from a slab structure, and discuss the viability for observing the node switching and flux expulsion phenomena previously discovered in lossless crystals.

DOI: 10.1103/PhysRevB.69.195111 PACS number(s): 71.36.+c, 42.70.Qs, 41.20.−q, 71.15.−m

I. INTRODUCTION

Recent advances[1,2] in the study of photonic crystals composed of materials which exhibit phonon-polariton excitations have revealed a variety of optical phenomena that are intimately related to the interplay between the strongly dispersive nature of these polar media and the structural dispersion of the crystal. These features involve (i) small frequency variations in bands with large regions of low group velocity that produce a polarization-dependent restructuring of the nodes in the field pattern (*node switching*) and (ii) transitions across the polariton gap boundary at the frequency ω_T that induce *flux expulsion* to and from the polariton material and the surrounding ambient dielectric. Previous polaritonic photonic crystal (PPC) band-structure simulations[1–6] have incorporated the polariton material as a lossless frequency-dependent dielectric. However, the node switching and flux expulsion phenomena are tied directly to the strong frequency dependence of the dielectric function near ω_T, where losses are expected to be greatest.

A simple model for the dielectric function of a polaritonic material with losses is[7]

$$\epsilon(\omega)=\varepsilon_\infty\left(1+\frac{\omega_L^2-\omega_T^2}{\omega_T^2-\omega^2-i\omega\gamma}\right), \tag{1}$$

where the magnitude of the losses is characterized by the width γ of the absorption peak in the imaginary part of ε. Previous considerations of the effects of losses in a PPC have been limited. Sigalas *et al.* implemented Eq. (1) in transmission calculations to determine the photonic band gaps in a PPC.[8] However, these simulations relied on a stepwise approximation to the dielectric function that disrupts the location of the flat bands near ω_T, which we have previously shown are sensitive to the rapid changes in dielectric function.[1,2] Several authors have also investigated the relationship between spatial and temporal decays in dissipative systems.[9,10]

The states of a periodic system where $\varepsilon(\mathbf{r})$ is complex are in general Bloch states with complex k and ω. Two subspaces of the total set of solutions are $\Phi_\omega=\{(k,\omega):\omega\in\Re\}$ and $\Phi_k=\{(k,\omega):k\in\Re\}$. The states with real frequency (Φ_ω) are accessible computationally using frequency-domain methods, such as the vectorial eigenmode expansion technique described in Sec. II, while the states with real-wave vector (Φ_k) can be obtained using a frequency-dependent time-domain method, which we introduce in Sec. III. These two methods solve fundamentally different problems. If the frequency is assumed to be real, the resulting wave decays in space, while the time-domain approach studies a real-wave-vector excitation that decays away in time. The solutions are identical only when ε is real. Throughout the remainder of this work, we will refer to the results of frequency-domain simulations as real-ω states/band structures and the results of time-domain simulations as real-k states/band structures. However, it is important to note that frequency-domain methods can compute states with complex ω as well.

In Sec. IV, we show that under certain conditions, the imaginary component of the wave vector of a real-ω state is related to the imaginary frequency component of a real-k state through a factor of the group velocity. In Sec. V, we analytically solve for real-ω and real-k states of a one-dimensional polaritonic photonic crystal. We compare the band-structure diagrams generated by the two methods, whose axes are $\mathrm{Re}[k]$ and $\mathrm{Re}[\omega]$. The real-k states sufficiently removed from ω_T have frequencies whose real parts are relatively unperturbed from the corresponding states of a lossless crystal, and the real-ω states that have wave vectors whose real parts are not close to the edge of the Brillouin zone closely agree with the position of the real-k states on the band-structure diagram. We find that these subsets of Φ_ω and Φ_k provide an ideal example of the aforementioned correspondence between the imaginary components of frequency and wave vector. However, the real-ω and real-k states with $\mathrm{Re}[k]$ near the edge of the Brillouin zone reveal few similarities, which can be attributed to the small group velocity at the band edges of the lossless crystal.

In Sec. VI, we find that the difference between the real-ω and real-k states in the band structure of a two-dimensional (2D) PPC is much more striking. As in the 1D crystal, the real-k band structure is qualitatively similar to the lossless crystal, which we have previously discovered exhibits the node switching and flux expulsion phenomena in the TE polarized bands for the given geometry.[1] As the width of the absorption loss peak increases, the real-ω bands begin to resemble the lowest band of the metallodielectric crystal that is obtained by replacing the polariton rod with a perfect metal. This is manifested by a folding back of the bands before they reach the Brillouin zone edge. This feature again occurs in frequency regimes associated with low group velocity in the lossless crystal.

Finally, in Sec. VII, we analyze the reflection and transmission of a plane-wave off of a slab consisting of five periods of the 2D PPC structure studied in Sec. VI. We find that such a source will excite real-ω states which exhibit the node switching and flux expulsion phenomena at relevant levels of loss, but the localization of the field is lower than for the corresponding real-k states. The reflection/transmission measurements in a computational experiment using the time-domain method agree with those using the frequency-domain method, as expected since the source excitation is the same in each. The reflectivity spectrum reveals the presence of *pseudogaps*: frequency ranges where the transmission drops but the reflectivity remains much less than 1. We attribute these features to the high loss states in the real-ω band structure that exist in the intervals representing the band gaps of the real-k band structure.

II. FREQUENCY-DOMAIN METHOD

Our previous studies of PPC band structures utilized a computational technique based on the vectorial eigenmode expansion.[2,11,1] This generic frequency-domain photonic simulation tool CAMFR (Refs. 11 and 12) can efficiently and accurately compute the Bloch states of a system with frequency-dependent dielectrics by dividing the unit cell into layers where the index profile does not change in the propagation direction. In each of these layers, we expand the field in the local eigenmodes of that particular layer. The only approximation is the size of the eigenmode basis, which we have determined to be well converged at 40.

Using mode matching, we derive frequency-dependent reflection and transmission matrices that completely describe the scattering behavior of the unit cell,

$$\mathbf{F}_2 = \mathbf{T}_{12}\cdot\mathbf{F}_1 + \mathbf{R}_{21}\cdot\mathbf{B}_2, \tag{2}$$

$$\mathbf{B}_1 = \mathbf{R}_{12}\cdot\mathbf{F}_1 + \mathbf{T}_{21}\cdot\mathbf{B}_2. \tag{3}$$

Here, $\mathbf{F}$ and $\mathbf{B}$ are column vectors containing the expansion coefficients of the forward and backward propagating fields, respectively. We then impose Bloch boundary conditions, and recast Eqs. (2) and (3) as a generalized eigenvalue problem, which can be solved for each frequency:

$$\begin{bmatrix} \mathbf{T}_{12} & \mathbf{R}_{21} \\ 0 & \mathbf{I} \end{bmatrix}\begin{bmatrix} \mathbf{F}_1 \\ q\mathbf{B}_1 \end{bmatrix} = q\begin{bmatrix} \mathbf{I} & 0 \\ \mathbf{R}_{12} & \mathbf{T}_{21} \end{bmatrix}\begin{bmatrix} \mathbf{F}_1 \\ q\mathbf{B}_1 \end{bmatrix},$$

where $\mathbf{I}$ is the unit matrix and $q = e^{-ika}$. Since the independent variable in these simulations is frequency, it is trivial to account for any frequency-dependent dielectric response.

III. TIME-DOMAIN METHOD

In a periodic time-domain approach, we solve the time-dependent Maxwell equations,

$$\nabla\times\mathbf{E} = -\mu\frac{\partial\mathbf{H}}{\partial t}, \nabla\times\mathbf{H} = \varepsilon_\infty\frac{\partial\mathbf{E}}{\partial t} + \frac{\partial\mathbf{P}}{\partial t},$$

where the electric polarization density $\mathbf{P}$ describes a forced oscillation at the phonon frequency ω_T with damping γ,[13,14]

$$\frac{d^2\mathbf{P}}{dt^2} + \gamma\frac{d\mathbf{P}}{dt} + \omega_T^2\mathbf{P} = \varepsilon_\infty(\omega_L^2 - \omega_T^2)\mathbf{E}. \tag{4}$$

Assuming a harmonic time dependence $\sim e^{-i\omega t}$ for both $\mathbf{E}$ and $\mathbf{P}$, Eq. (4) results in an effective dielectric function $\varepsilon = \varepsilon_1 + i\varepsilon_2$ that matches precisely with Eq. (1),

$$\varepsilon_1 = \varepsilon_\infty\left[1 + \frac{(\omega_L^2-\omega_T^2)(\omega_T^2-\omega^2)}{(\omega_T^2-\omega^2)^2 + \omega^2\gamma^2}\right],$$

$$\varepsilon_2 = \varepsilon_\infty\frac{(\omega_L^2-\omega_T^2)\omega\gamma}{(\omega_T^2-\omega^2)^2 + \omega^2\gamma^2}.$$

A Bloch state is generated with real-wave vector using a periodic source that produces a propagating wave which decays in time. We note that due to losses, it is necessary to perform several simulations, each with sources based around different center frequencies spread throughout the frequency range of interest in the band structure.

Given finite grid spacing, $\varepsilon(\omega) = n(\omega)^2$ can be derived from the electric fields at two points separated by a distance x_{12} using the relation

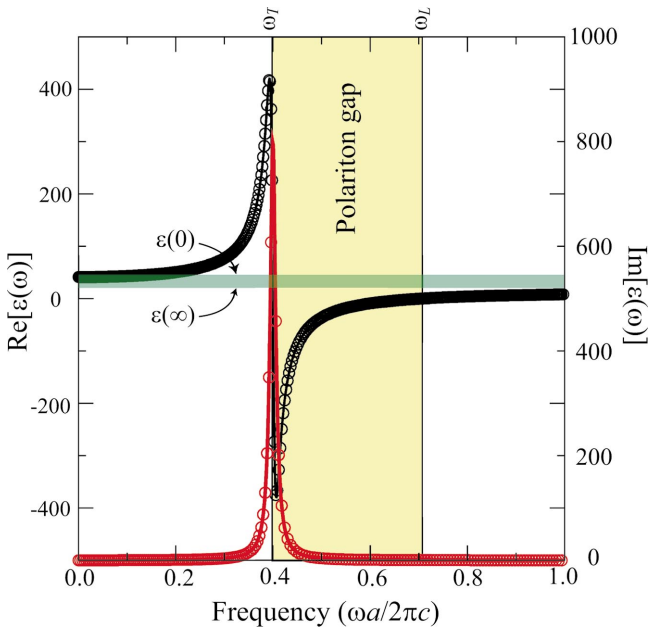

FIG. 1. (Color) The polariton dielectric function for $LiTaO_3$ with $\varepsilon_\infty = 13.4$ and $a = 4.5\ \mu$m, leading to normalized frequencies $\omega_T = 0.4$, $\omega_L = 0.703$, and $\gamma = 0.014$. The real part ε_1 is in black and the imaginary part ε_2 is in red. Note the excellent agreement between the exact value from Eq. (1) used in frequency-domain simulations (solid line) and approximate value derived from time-domain simulations with $a = 160$ grid points using Eq. (5) (circular symbols).

$$n(\omega) = \frac{i}{2\pi\omega x_{12}} \ln \frac{E_2(\omega)}{E_1(\omega)}. \tag{5}$$

A comparison between the approximate results of Eq. (5) applied to a bulk real-k simulation with $a = 160$ grid points and the exact value from Eq. (1) used in real-ω simulations is given in Fig. 1.

IV. RELATIONSHIP BETWEEN REAL ω AND REAL k STATES

We now consider the general problem of comparing real-frequency and real-wave vector states in lossy systems. A general Bloch state is a solution to the master equation $f(k,\omega) = 0$ of the form $(k_1 + ik_2, \omega_1 + i\omega_2)$. Consider a point (k_0, ω_0) with $k_0, \omega_0 \in$ Re. Then,

$$f(k,\omega) = f(k_0,\omega_0) + (k-k_0)\left.\frac{\partial f}{\partial k}\right|_{k_0,\omega_0} + (\omega-\omega_0)\left.\frac{\partial f}{\partial \omega}\right|_{k_0,\omega_0} + \mathcal{O}_2[(k-k_0),(\omega-\omega_0)], \tag{6}$$

where $\mathcal{O}_2(x,y)$ refers to terms of second order in x and/or y. Assuming they exist, we consider two solutions of the master equation, $(k_0, \omega_0 + \Delta\omega_1 + i\Delta\omega_2)$ and $(k_0 + \Delta k_1 + i\Delta k_2, \omega_0)$, with $\Delta\omega_{1,2}, \Delta k_{1,2} \in \Re$. Ignoring second-order terms in Eq. (6),

$$-f(k_0,\omega_0) = (\Delta k_1 + i\Delta k_2)\left.\frac{\partial f}{\partial k}\right|_{k_0,\omega_0},$$

$$-f(k_0,\omega_0) = (\Delta\omega_1 + i\Delta\omega_2)\left.\frac{\partial f}{\partial \omega}\right|_{k_0,\omega_0}.$$

Therefore,

$$\left.\frac{\partial \omega}{\partial k}\right|_{k_0,\omega_0} \equiv -\left.\frac{\partial f}{\partial k}\right/\left.\frac{\partial f}{\partial \omega}\right|_{k_0,\omega_0} = -\frac{\Delta\omega_1 + i\Delta\omega_2}{\Delta k_1 + i\Delta k_2}. \tag{7}$$

Equation (7) states that if the real-ω and real-k band structures coincide at a particular $(k_0,\omega_0) \in \Re$ ($\Delta\omega_1, \Delta k_1 \approx 0$), then the imaginary components Δk_2 and $\Delta\omega_2$ are related by a factor of the group velocity,

$$\Delta\omega_2 = -\Delta k_2 \left.\frac{\partial \omega}{\partial k}\right|_{k_0,\omega_0} \equiv -\Delta k_2 v_g. \tag{8}$$

This also demonstrates that the group velocity as defined by Eq. (7) is purely real at (k_0,ω_0) in this system. We note that this argument implicitly assumes that losses are small ($n_2 \ll n_1$) so that the perturbations to k and ω are small compared with (k_0,ω_0). These results are independent of the dimensionality of the photonic crystal; however, the validity of Eq. (8) ultimately rests on the applicability of the assumption $\Delta\omega_1 = \Delta k_1 = 0$. The factor of v_g can be understood by comparing the nature of the real-k and real-ω states. A real-k state has fields with no spatial decay and is unaffected by the group velocity, unlike real-ω states with complex k that decay spatially and hence will be affected more strongly by the lossy polariton material when v_g is small.

Previous work[10,9] has argued that the relationship in Eq. (8) holds for small losses. In particular, Krohkin and Halevi (KH) follow a similar analysis using Taylor expansion of the master equation, but with less generality. In order to arrive at Eq. (8), KH implicitly assume that a pair of Bloch states exists with $\Delta\omega_1 = \Delta k_1 = 0$. In the following section, we will demonstrate that in a 1D PPC, this condition holds for the lowest few bands, except very close to the band edges.

However, in a bulk system where $k = n\omega/c$, it is easy to show that Eq. (8) *does not* hold, even for small losses. A solution of the form $(k_0 + i\Delta k_2, \omega_0)$ satisfies $k_0 = n_1\omega_0/c$ and $\Delta k_2 = n_2\omega_0/c$. Therefore,

$$\Delta k_2 = k_0 \frac{n_2(\omega_0)}{n_1(\omega_0)}. \tag{9}$$

The only solution of the form $(k_0, \omega_0 + \Delta\omega_1 + i\Delta\omega_2)$ is

$$\Delta\omega_1 = -\left.\frac{ck_0}{n_1}\right|_{\omega_0} + ck_0 \left.\frac{n_1}{n_1^2 + n_2^2}\right|_{\omega_0 + \Delta\omega_1 + i\Delta\omega_2} \tag{10}$$

$$\Delta\omega_2 = -ck_0 \left.\frac{n_2}{n_1^2 + n_2^2}\right|_{\omega_0 + \Delta\omega_1 + i\Delta\omega_2}. \tag{11}$$

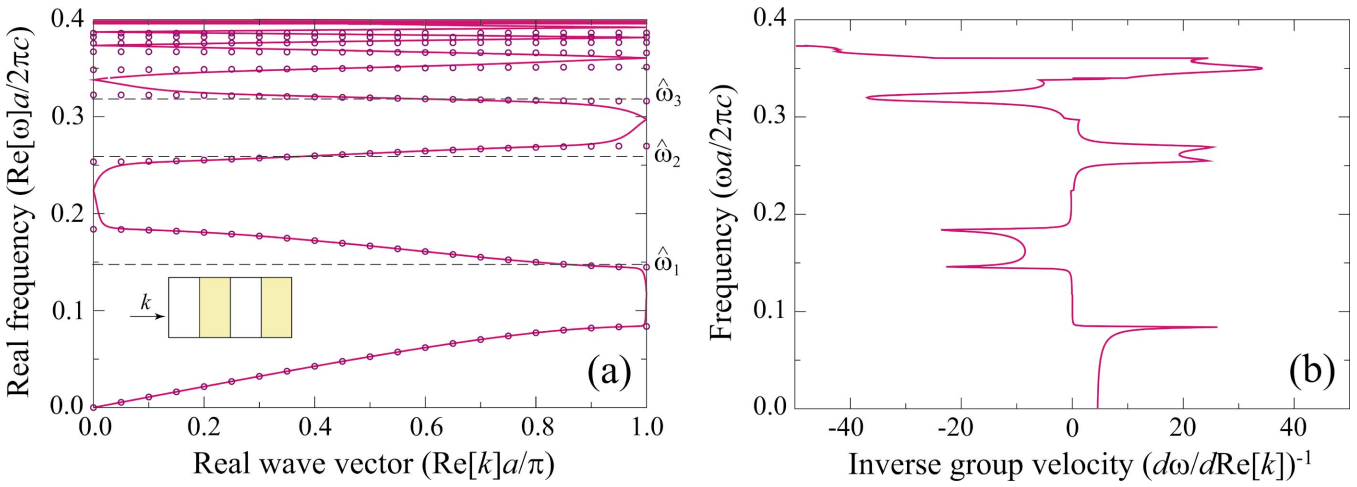

FIG. 2. (Color) Lossy one-dimensional PPC structures: (a) Comparison of band-structure calculations for the 1D lossy $LiTaO_3$ PPC shown in the inset using frequency-domain and time-domain approaches. The solid pink line is the real part of the wave-vector solution assuming real frequency in Eq. (14), while the purple circular symbols are the real part of the frequency solution assuming real-wave vector. Note the presence of frequency gaps only when k is purely real, and coincidence of the two methods in the middle of the Brillouin zone. (b) The inverse of the "group velocity" defined by $\tilde{v}_g^{-1}=(d\omega/d\,\mathrm{Re}[k])^{-1}$ as calculated from the real-ω simulation.

If we can assume that $n(\omega_0)\approx n(\omega_0+\Delta\omega_1+i\Delta\omega_2)$ (as would be the case, e.g. in a frequency-independent dielectric material) we can combine Eqs. (9) and (11),

$$\Delta\omega_2=-c\Delta k_2\frac{n_1}{n_1^2+n_2^2}=-\Delta k_2\mathrm{Re}\left[\frac{\partial\omega}{\partial k}\right], \tag{12}$$

since $\partial\omega/\partial k=c/n$. This result holds even for large Δk_2 and $\Delta\omega_2$. We see that because $\Delta\omega_1$ in Eq. (10) is no longer zero, it is only the real part of the group velocity which transforms between Δk_2 and $\Delta\omega_2$. We note that this conclusion comes from the natural pairing of states with the same real wave vector component and comparing the shift in frequency. A similar analysis assuming $\Delta\omega_1=0$ produces

$$\Delta\omega_2=-c\Delta k_2/n_1. \tag{13}$$

The difference between Eqs. (12) and (13) stems from the fact that when it is impossible to simultaneously choose $\Delta k_1=0$ and $\Delta\omega_1=0$, there is no logical pairing of real-k and real-ω states for which to apply Eq. (8). We will present a more striking example of this situation in a 2D PPC in Sec. VI.

V. 1D CRYSTALS

The one-dimensional PPC problem is useful because it is analytically solvable. We consider a system of air and $LiTaO_3$ a material with a large polariton gap from $\omega_T=26.7$ THz to $\omega_L=46.9$ THz, $\varepsilon_\infty=13.4$, and $\gamma=0.94$ THz. We set $a=4.5$ μm so that $\omega_T=0.4(2\pi c/a)$, and $\gamma=0.014(2\pi c/a)$. The slabs have width $d_1=d_2=a/2$. The Bloch states are given by solutions of

$$\cos(ka)=\cos\left(\frac{\omega d_1}{c}\right)\cos\left(\frac{n(\omega)\omega d_2}{c}\right)-\frac{1+n(\omega)^2}{2n(\omega)}\sin\left(\frac{\omega d_1}{c}\right)\sin\left(\frac{n(\omega)\omega d_2}{c}\right), \tag{14}$$

which is solvable through inversion for k if ω is given and through Newton's method for ω if k is given. We note that although Eq. (14) is generally referred to in the context of a frequency-domain problem, it is in fact a general solution to

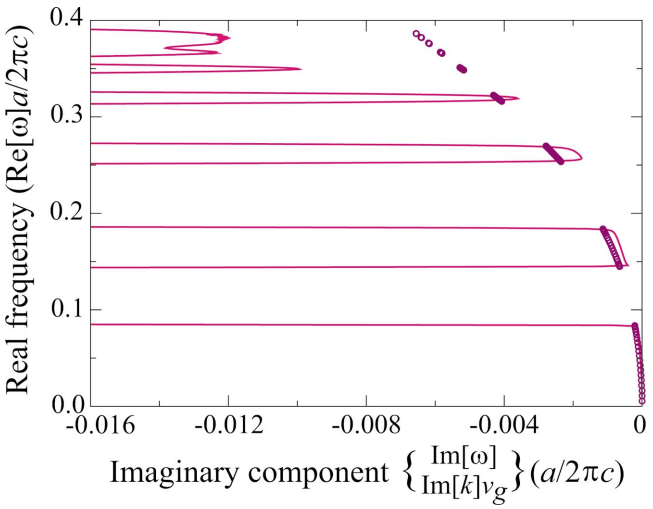

FIG. 3. (Color) Comparison of the imaginary components of the band-structure calculations in Fig. 2. In purple circular symbols is the imaginary part of the frequency when the wave vector is assumed to be real, while the pink line is the imaginary part of the wave vector when the frequency is assumed to be real, rescaled by the quantity $\tilde{v}_g$. Note the agreement in the first three bands, simultaneous with the coincidence of the band-structure diagrams as described in Sec. IV.

the arbitrary 1D Bloch boundary value problem for a plane wave with complex k and/or ω. We plot the real component of the solutions assuming either real frequency or real-wave vector in Fig. 2(a). To stress the low ''group velocity'' of the higher bands, the inverse $1/\tilde{v}_g=(d\omega/d\mathrm{Re}[k])^{-1}$ obtained from the real-ω solutions is shown in Fig. 2(b). Near the band edges, the two methods produce differing results. When k is real, there are gaps where no Bloch solution exists whose frequency has a real component within these frequency ranges. However, the band structure for real ω is a continuous line, with a solution lying somewhere within the Brillouin zone for all ω.

Nevertheless, the real-k and real-ω bands show excellent agreement in the middle of the Brillouin zone. Therefore, we can choose states such that $\Delta\omega_1\approx 0$ and $\Delta k_1\approx 0$ simultaneously, and the coinciding states $(k_0+i\Delta k_2,\omega_0)$ and $(k_0,\omega_0+i\Delta\omega_2)$ should be related by a factor of the group velocity. In Fig. 3, we compare the values of $\mathrm{Im}[\omega]$ and $\mathrm{Im}[k]v_g$ as functions of $\mathrm{Re}[\omega]$. Equation (8) holds extremely well through the first few bands, showing disagreement only close to ω_T when the terms of second order in Δk_2 in Eq. (6) can no longer be ignored and the two band structures cease to coincide. As ω increases, the group velocity becomes much smaller than c,[2] and so the imaginary wavevector component from real-ω calculations is several orders of magnitude larger than the imaginary frequency component from real-k calculations.

As is the case for lossless crystals,[2] the frequencies of the bands of the 1D PPC at the midpoint of the Brillouin zone show excellent agreement with the resonance frequencies given by solutions to

$$\hat{\omega}_j=j\pi c/dn_1(\hat{\omega}_j), \tag{15}$$

where d is the width of the polariton slab(rod). Note that unlike the lossless crystal, there are only a finite number of solutions to Eq. 15 with real ω since $\varepsilon(\omega)$ no longer blows up at ω_T. We list these frequencies, as well as the value of the dielectric function at $\hat{\omega}_j$, in Table I.

TABLE I. Comparison of the band frequencies at $k=\pi/2a$ to $\hat{\omega}_j$ from Eq. (15) for a 1D PPC of $LiTaO_3$ slabs in air with $d_1=d_2=a/2$. In the last column is the value of ε at $\omega=\hat{\omega}_j$. The resonance at $\hat{\omega}_9$ does not have a corresponding band in the PPC.

m	$\omega(\pi/2a)$	$\hat{\omega}_j$	$\varepsilon(\hat{\omega}_j)$
1	0.1667	0.1478	$45.81+0.4882i$
2	0.2622	0.2564	$60.84+1.817i$
3	0.3194	0.3179	$88.95+5.737i$
4	0.3498	0.3498	$130.4+15.31i$
5	0.3664	0.3671	$183.7+34.88i$
6	0.3761	0.3775	$247.8+71.21i$
7	0.3822	0.3843	$318.2+134.0i$
8	0.3863	0.3893	$386.5+242.2i$
9	N/A	0.3943	$408.5+484.5i$

VI. 2D CRYSTALS

We can apply the insights from Secs. IV and V to the band structures of a two-dimensional polaritonic photonic crystal, computed using either the frequency-domain or time-domain method. We consider a 2D photonic crystal of square rods in air with sides of length s ($s/a=0.25$) in a square lattice. The rods are taken to be $LiTaO_3$, with $a=4.5$ μm so that $\omega_T=0.4(2\pi c/a)$, $\omega_L=0.703(2\pi c/a)$ and $\gamma=0.014(2\pi c/a)$.

In Fig. 4, we plot the band structure from Γ-X-M-Γ computed using the time-domain method from Sec. III. We overlay with dashed lines the band structure for the metallodielectric crystal obtained by replacing $LiTaO_3$ with a perfect metal. Similar to a lossless crystal,[1,2] both the TE and TM bands are relatively flat in most frequency regions below ω_T, where they resemble rod-localized resonance modes. We again note the finite number of bands, related to the finite maximum in ε introduced by the absorption peak. The TE bands also display an anticrossing interaction related to the existence of Bloch states of the geometrically equivalent metallodielectric crystal. There is very little perturbation from the band structure of the lossless crystal for the bands shown. This is because the frequency is always many factors of γ away from ω_T, where $\varepsilon_2\ll\varepsilon_1$. In this regime, the shape of $\varepsilon_1(\omega)$, and hence the spatial modulation of the Bloch state, are virtually unchanged.

Like the lossless crystal, PPC states of TE polarization exist with real component of frequency both below and above ω_T, even at frequencies very close to ω_T. This allows for the realization of the node switching phenomenon through a variety of field profiles and the flux expulsion phenomenon over a frequency range down to a few γ. We note that as the dielectric function makes a rapid transition from high index to metallic around ω_T, the TE band inside the polariton gap appears discontinuously as in the lossless crystal.[2] In addition, for frequencies within $\sim\gamma$ of ω_T, the polariton material is too lossy to observe any states on the same time scales that were used to generate the rest of the band-structure diagram. The two experimental phenomena that were previously introduced in a lossless crystal[1] can easily be realized in the lossy crystal. In Figs. 5(a) and 5(b), we demonstrate node switching through the high localization of the fields at the edges of the second TE-polarized band, which connects the $TE_{1,1}$ rod-localized state to the $TE_{1,2}$ state. In Fig. 5(c), we verify the existence of states above ω_T by showing a state with fields that are essentially expelled from the polaritonic region.

We found in Sec. V that the real-ω band structure of the 1D PPC differed from the real-k band structure near the band edges, where the group velocity is smallest. An additional feature is introduced in two-dimensional PPCs that further distinguishes the real-ω and real-k states in the regions of low group velocity. The existence of a lossless band ($\mathrm{Im}[k]=0$) in the metallodielectric crystal in the frequency range below ω_T introduces the possibility that light can choose to circumvent the lossy polariton rods and concentrate flux in the ambient region. The PPC reveals precisely this tendency in the real-ω band structure in Fig. 6, where we plot the TE-polarized state at each real frequency with the

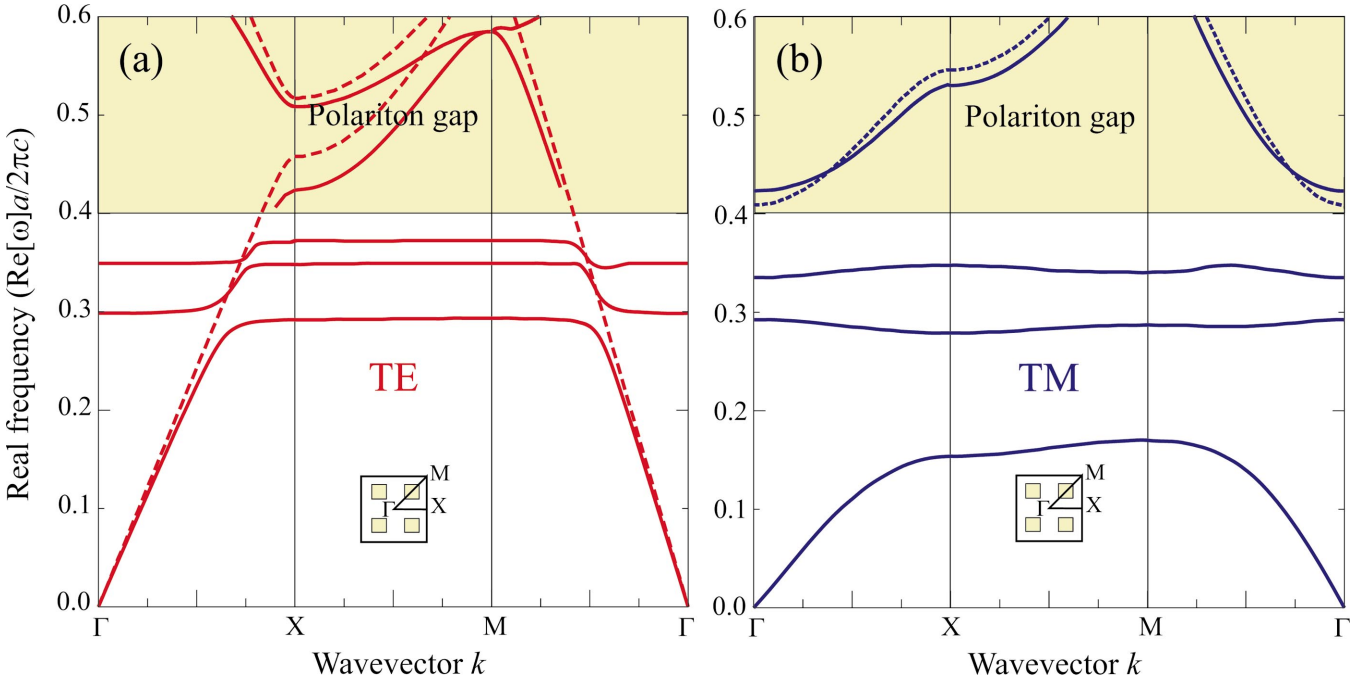

FIG. 4. (Color) Band structure of a square 2D PPC of square $LiTaO_3$ rods in air with sides of length $s/a=0.25$, $\omega_T=0.4(2\pi c/a)$, $\omega_L=0.703(2\pi c/a)$, $\varepsilon_\infty=13.4$, and $\gamma=0.014(2\pi c/a)$ along the edge of the irreducible Brillouin zone from Γ to X to M to Γ, calculated using frequency-dependent time-domain simulations. The TE (**H** out-of-plane) bands are in red in (a), TM (**E** out-of-plane) in blue in (b). At distances greater than γ away from ω_T, this band structure shows little difference qualitatively from that of the crystal of lossless polaritonic material ($\gamma=0$) (Ref. 1). The TE(TM) bands of a metallodielectric crystal obtained by replacing $LiTaO_3$ by a perfect metal are given by the red(blue) dashed lines.

lowest imaginary-wave-vector component for the same crystal structure used in Fig. 4. We vary the absorption peak width γ between $0.0001(2\pi c/a)$ and $0.01(2\pi c/a)$ and concentrate on the locations of the first three photonic band gaps in the real-k band structure. The bands are obtained by selecting the Bloch wave vector at each frequency with the smallest absolute value of Im[k].

As γ increases to $\sim 0.01(2\pi c/a)$, the band structure takes on a strikingly different character. In particular, the anticrossing interaction with the localized rod states that produced the flat band regions in the lossless crystal becomes greatly reduced, and the bands fold back and connect within the regions marked in purple shading that correspond to the bandgaps of the real-k simulations. This surprising band back-bending, with two superluminal points of infinite group velocity in each band gap, has also been observed in constant dielectric simulations with complex ϵ (Ref. 15) and at surface plasmon resonances.[16] The superluminal behavior can be attributed to the remnants of the photonic band gaps,[17] and is found only in frequency ranges where the imaginary component of the wave vector is prohibitively large. In the context of Sec. IV, it is clear that in a 2D crystal the assumption of the existence of states with $\Delta k_1, \Delta\omega_1 \approx 0$ and $\Delta k_2, \Delta\omega_2$ small breaks down entirely, and Eq. (8) is no

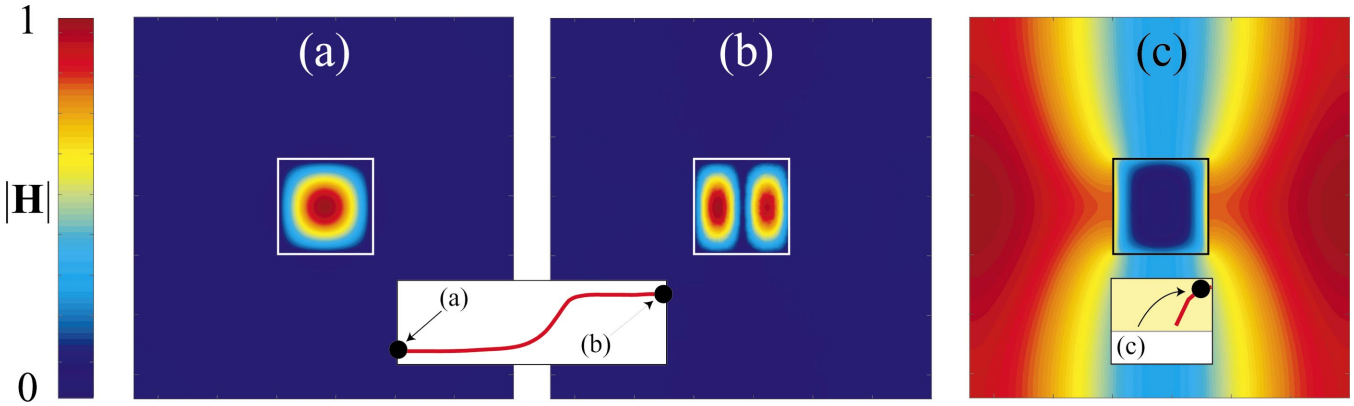

FIG. 5. (Color) Magnetic field profiles ($|\mathbf{H}|$) of the TE-polarized states at three representative points on the band structure diagram in Fig. 4. (a) [$\omega=0.3(2\pi c/a), k=\Gamma$] and (b) [$\omega=0.355(2\pi c/a), k=\mathrm{X}$] show the field localization at the band edges of the second band. (c) [$\omega=0.44(2\pi c/a), k=0.475(2\pi/a)$] shows the metallic profile above ω_T.

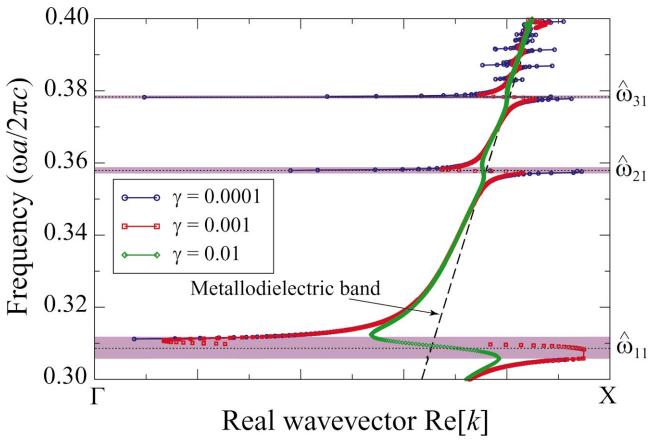

FIG. 6. (Color) Band structure from Γ to X of the same crystal as in Fig. 4 calculated using real-ω simulations, with the loss parameter γ varied from $0.0001(2\pi c/a)$ to $0.01(2\pi c/a)$. As γ increases to $0.01(2\pi c/a)$, the first bands clearly fail to extend to the edges of the Brillouin zone. Instead, the band structure begins to mimic the lowest TE-polarized metallodielectric band, shown as a dashed solid line. The imaginary component of wave vector (not shown) increases sharply in the gaplike regions marked in purple.

longer relevant. We expect that if corresponding states around $k=\Gamma$ and $k=\mathrm{X}$ with real frequency were to exist in the real-ω band structure, they would exhibit prohibitively high losses, due to the low group velocity of the corresponding bands of the lossless crystal near the resonance frequencies.

We have also marked the locations of the rod resonance frequencies $\hat{\omega}_{11}=0.311(2\pi c/a)$, $\hat{\omega}_{21}=0.359(2\pi c/a)$, and $\hat{\omega}_{31}=0.380(2\pi c/a)$ solving $\hat{\omega}_{ij}=\sqrt{i^2+j^2}\pi c/sn_1$, which all lie within the band gap regions [$\hat{\omega}_{22}=0.374(2\pi c/a)$ does not interact with the metallodielectric band due to symmetry

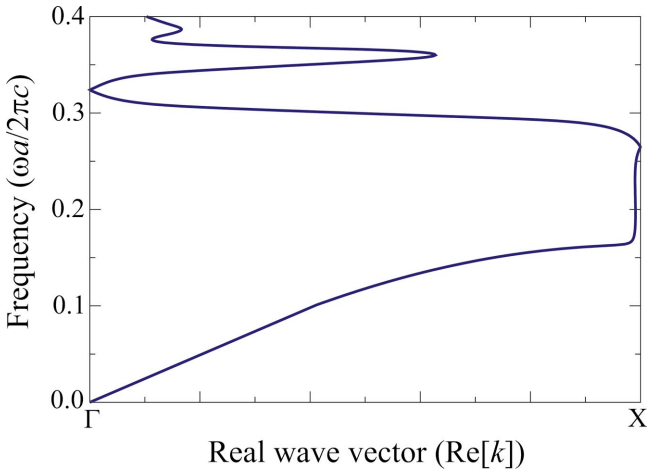

FIG. 7. (Color) TM bands of the 2D $LiTaO_3$ crystal with $\gamma=0.014(2\pi c/a)$ from a real-ω simulation. Note the similarities in appearance of the first few bands to the bands of the 1D PPC in Fig. 2(a). The bands are flat, except near the band edges. Moreover, despite the fact that the bands extend from $k=\Gamma$ to $k=\mathrm{X}$, there are no band gaps.

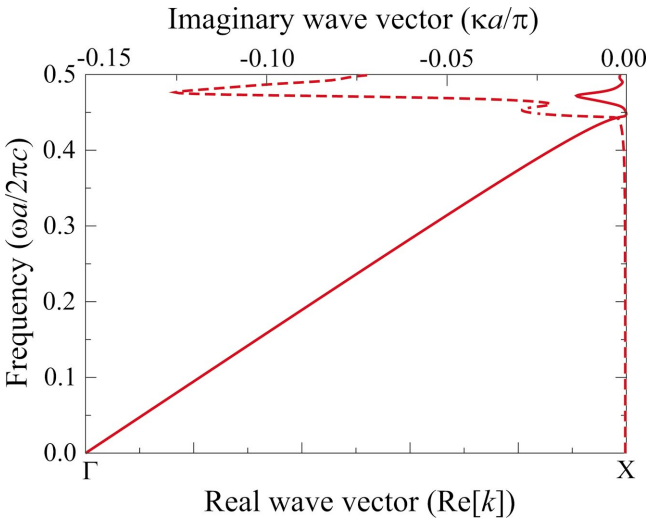

FIG. 8. (Color) Real (solid) and imaginary (dashed) wave-vector components from a real-ω simulation of the TE bands of a crystal of square SiC rods with $s/a=0.25$, $\varepsilon_\infty=6.7$, $\omega_T=0.5(2\pi c/a)$, $\omega_L=0.6(2\pi c/a)$, and $\gamma=0.01(2\pi c/a)$. Note that the modes remain close to the edge of the Brillouin zone at frequencies near ω_T, unlike the lossless crystal which has flat bands extending from Γ to X.

considerations[2]]. The only other resonance mode of this system with real frequency is $\hat{\omega}_{32}=0.386(2\pi c/a)$.

We associate the features of the $\gamma\sim 0.01(2\pi c/a)$ real-ω band structure with the tendency of the light to prefer the metallodielectric configuration with the flux predominantly expelled from the polariton region. We find a different situation entirely when studying the TM-polarized bands of the $LiTaO_3$ crystal. Because ω_T is below the lower edge of the fundamental TM band gap of the metallodielectric crystal, the bands plotted in Fig. 7 with $\gamma=0.014(2\pi c/a)$ appear similar qualitatively to those of the 1D crystal since the metallodielectric bands play no role.

As further evidence of the influence of the metallodielectric crystal states, we can shift the resonance frequencies into the TE band gap of the metallodielectric crystal by shifting ω_T through a change in a. In Fig. 8, we plot the TE bands of a 2D PPC of SiC rods with $s/a=0.25$, $\varepsilon=6.7$, $\omega_T=0.5(2\pi c/a)$, $\omega_L=0.6(2\pi c/a)$, and $\gamma=0.01(2\pi c/a)$ (a purely speculative amount of loss for this material). The lowest resonance frequency $\hat{\omega}_{11}$ is now inside the band gap of the metallodielectric crystal [cf. Fig. 4(a)]. Due to the lack of an anticrossing interaction, the bands of the lossless crystal are very flat in the middle of the Brillouin zone. It is now modes with real component of k away from the edges of the Brillouin zone that would have prohibitively large imaginary component due to the low group velocity in the lossless crystal near these frequencies. The result is that instead of the flat band near $\omega=0.473(2\pi c/a)$ that extends from Γ to X in the lossless crystal, the states with lowest loss occur only near the wave vector $k=\mathrm{X}$. This effect can also be observed in the behavior of the TM states near ω_T in Fig. 7, which are clustered around $k=\Gamma$.

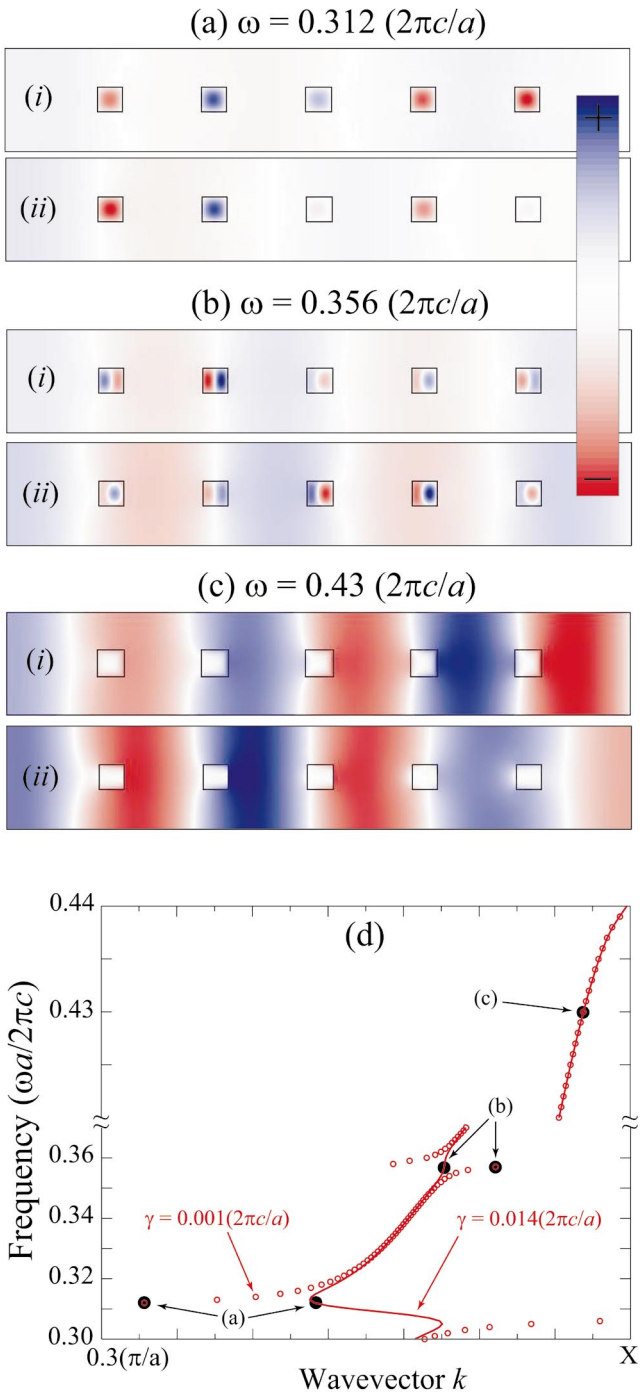

FIG. 9. (Color) Magnetic field profiles ($|\mathbf{H}|$) of TE-polarized modes excited in a slab of five periods of a 2D $LiTaO_3$ crystal by a plane-wave for two different absorption peak widths: (i) $\gamma = 0.001(2\pi c/a)$ and (ii) $0.014(2\pi c/a)$. (a) $\omega = 0.312(2\pi c/a)$ and (b) $\omega = 0.356(2\pi c/a)$ show the field localized inside the rod at wave vectors near the edges of the Brillouin zone and represent the node switching phenomenon. Note that the rod localization of the fields for becomes steadily worse as γ increases due to the increasing preference for a metalliclike configuration. In (a)–(ii), the reduction in rod localization is very slight since ω is far away from ω_T; the change in field profile is due to the fact that the wave vector is shifted by $0.225\pi/a$. (c) The field profile at $\omega = 0.44(2\pi c/a)$ is highly metallic, and in combination with the states in (b) verifies the existence of the flux expulsion phenomenon. (d) The states of the infinite crystal corresponding to the modes in (a)–(c) identified on a real-ω band-structure diagram by black dots.

VII. RELEVANCE TO EXPERIMENTAL MEASUREMENTS

The question of experimental accessibility arises for the two classes of states discussed above. A previous experiment using the coherent microwave transient spectroscopy (COMITS) technique excited particular Bloch states of a 2D crystal using a plane-wave source.[18] Since the frequency is conserved in the transmission of a plane wave through a slab structure, we expect that only the real-ω states will be excited in this type of experiment if it involves a system with losses.

To simulate the results of a COMITS experiment which probes the node switching and field expulsion phenomena, we use CAMFR to examine the field profile of the real-ω mode excited in a slab of five periods of the $LiTaO_3$ crystal structure from Sec. VI by a plane wave at frequencies similar to those studied in Fig. 5. At frequencies below ω_T, we expect that relatively few periods are necessary to generate the highly localized states of the system near the resonance frequencies. In Figs. 9(a) and 9(b), we demonstrate node switching at frequencies near the $TE_{1,1}$ and $TE_{1,2}$ resonances using two different values of γ: $\gamma_1 = 0.001(2\pi c/a)$ and $\gamma_2 = 0.014(2\pi c/a)$. We compare the actual level of loss (γ_2) to a smaller value γ_1 in order to study the intermediate changes in the fields between a physical $LiTaO_3$ crystal with

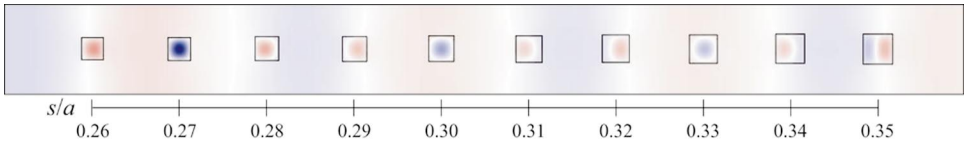

FIG. 10. (Color) Magnetic field profile ($|\mathbf{H}|$) of a TE-polarized mode excited in a slab of 10 periods of a 2D $LiTaO_3$ crystal by a plane-wave of frequency $\omega=0.312(2\pi c/a)$ where $\omega_T=0.4(2\pi c/a)$, $\gamma=0.014(2\pi c/a)$, and the width of the rods is slowly increased from $s=0.26a$ to $0.35a$ in steps of $0.01a$. Note the transition from the $\hat{\omega}_{11}$ to the $\hat{\omega}_{21}$ resonance mode.

losses and the lossless crystals previously examined.[1] As γ increases, the rod localization of the field clearly decreases as the frequency approaches ω_T and the field configuration becomes more metallic. In Fig. 9(c), we demonstrate flux expulsion from the polariton rod using an incident wave with $\omega>\omega_T$. The states of the infinite crystal at the frequencies of interest are identified on a band structure in Fig. 9(d). Above ω_T, the band structure is virtually unaffected by the amount of loss, since most of the field is removed from the polariton region. We note that the node switching phenomenon can also be observed at fixed frequency. In Fig. 10, we consider a polaronic crystal slab with 10 periods of a square $LiTaO_3$ rod in air that increases in width from $s=0.26a$ to $0.35a$ in steps of $0.01a$. As the rods increase in size, the resonance frequencies of the rods decrease. The effect is the same as moving along one of the bands of the PPC. With $\omega_I=0.4\pi c/a)$ and $\gamma=0.014(\pi c/a)$, an incident plane wave at $\omega=0.312(2\pi c/a)$ first excites the $\hat{\omega}_{11}$ resonance mode and then smoothly transitions to the $\hat{\omega}_{21}$ mode along the slab.

In order to observe the propagating states with real-wave vector that are generated in a real-k band-structure calculation, it may be necessary to mimic the periodic source conditions of our simulations. This could be possible by coupling to a state in Φ_k through a grating on the surface of the photonic crystal. These states decay relatively slowly, even near the band edges where the full width at half maximum is at most 50% greater than the states in the middle of the Brillouin zone. If these modes can be excited, the node switching and flux expulsion phenomena can be observed at higher levels of loss with more field localization than is possible using real-ω states.

We mention that the frequency regimes without states in the real-k band structure are not true band gaps, because they lack the high reflectivity characteristic of a lossless photonic band gap.[8] In fact, any crystal with absorptive materials cannot produce the perfect interference of reflected waves through Bragg scattering that is considered to produce a normal gap in a lossless crystal. In Fig. 10, we compare the reflection and transmission of a plane wave off of the same five-layer slab structure studied in Fig. 9 at frequencies near the gaplike regions (*pseudogaps*) using both the time-domain and frequency-domain methods. As expected, they show good agreement since the simulations are reproducing the same computational experiment. From the perspective of the real-ω band structure, this drop in transmission without a correspondingly high reflectivity can be attributed to coupling to the high-loss real-ω states that exist within the pseudogap regions. Figure 10 demonstrates that the maximum value of the reflectivity in the pseudogap regions clearly decreases as the frequency approaches the absorption peak at $\omega_T=0.4$ and the magnitude of $\mathrm{Im}[k]$ within the pseudogaps increases.

VIII. CONCLUSION

In conclusion, we have extended our investigations of the optical phenomena in PPCs to lossy crystals, and presented a formalism for understanding the two classes of states, Φ_ω (real frequency) and Φ_k (real-wave vector). In a 1D PPC, we have found that due to the coincidence of the real-ω and real-k band structures, the time decay represented by the imaginary frequency component of the real-k states is related to the spatial decay represented by the imaginary-wave-vector component of the real-ω state with the same real-wave vector and frequency components through a factor of the group velocity (see Fig. 11).

However, as the width of the absorption peak increases, the real-ω band structure of a 2D PPC consisting of square $LiTaO_3$ rods diverges from the real-k band structure, which

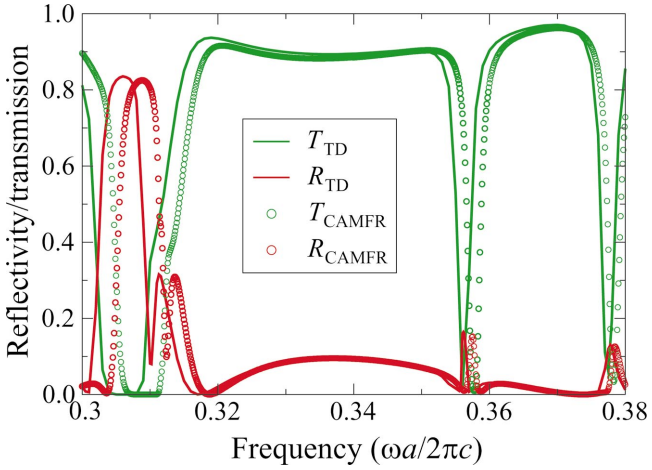

FIG. 11. (Color) Reflectivity and transmission off five layers of a 2D square PPC of square $LiTaO_3$ rods with $\gamma=0.001(2\pi c/a)$. The reflectivity is shown in red, the transmission in green, Real-ψ simulations with 40 eigenmodes are shown with circular symbols, real-k simulations with $a=160$ grid points are shown with solid lines. Note the pseudogap regions near the center frequencies of $0.309(2\pi/a)$ and 0.357 $(2\pi c/a)$, where the transmission shows a marked decrease. The reflectivity in these frequency ranges is much lower than 1, and in fact displays no noticeable features near the second pseudogap for $\gamma=0.014$ (not shown). The small shift ($\sim$0.5%) between the two data sets is due to the fact that the results of time-domain simulations coverge from below as a function of the grid resolution, while the results of frequency-domain simulations coverge from above as a function of the number of eigenmodes.

is relatively unperturbed from previous simulations for a lossless crystal,[1] as the absorption peak width γ increases. Any states near the edges of the Brillouin zone could only exist with extremely high spatial decay rates, which we associate with the low group velocity. Instead, the states with lowest loss are metalliclike with high localization in the surrounding ambient dielectric region, exhibited in the band structure by a folding of the bands before they reach Γ or X. As γ reaches the experimentally measured value for $LiTaO_3$, the entire real-ω band structure below ω_T closely resembles that of a metallodielectric crystal with the polariton rods replaced by a perfect metal.

Our analysis applies equally well to the broader class of periodic structures containing any lossy materials, not only polaritonic media. Ultimately, we conclude that both computational techniques used in this work provide accurate and efficient means to solve for two distinct classes of states. The variables which effect the similarities between these two sets extends beyond simply the absorption peak width γ, but rather also depends strongly on the geometry of the structure. In this light, the distinction between real-k and real-ω states must also be considered in experiments when attempting to reproduce theoretical predictions in lossy systems.

ACKNOWLEDGMENTS

K.C.H. would like to thank Chiyan Luo and Michelle Povinelli for many useful discussions. Funding was provided by the MRSEC program of the NSF under Grant No. DMR-0213282. P. B. acknowledges support from the Flemish Fund for Scientific Research (FWO-Vlaanderen).

*Electronic address: kch23@mit.edu

[1] K.C. Huang, P. Bienstman, J.D. Joannopoulos, K.A. Nelson, and S. Fan, Phys. Rev. Lett. **90**, 196402 (2003).
[2] K.C. Huang, P. Bienstman, J.D. Joannopoulos, K.A. Nelson, and S. Fan, Phys. Rev. B **68**, 075209 (2003).
[3] W. Zhang, A. Hu, X. Lei, N. Xu, and N. Ming, Phys. Rev. B **54**, 10 280 (1996).
[4] V. Kuzmiak, A.A. Maradudin, and A.R. McGurn, Phys. Rev. B **55**, 4298 (1997).
[5] A.Y. Sivachenko, M.E. Raikh, and Z.V. Vardeny, Phys. Rev. A **64**, 013809 (2001).
[6] N. Eradat, A.Y. Sivachenko, M.E. Raikh, and Z.V. Vardeny, Appl. Phys. Lett. **80**, 3491 (2002).
[7] C. Kittel, *Introduction to Solid State Physics* (Wiley, New York, 1976).
[8] M.M. Sigalas, C.M. Soukoulis, C.T. Chan, and K.M. Ho, Phys. Rev. B **49**, 11 080 (1994).
[9] A.A. Krokhin and P. Halevi, Phys. Rev. B **53**, 1205 (1996).
[10] T. Ochiai and K. Sakoda, Phys. Rev. B **64**, 045108 (2001).
[11] P. Bienstman and R. Baets, Opt. Quantum Electron. **33**, 327 (2001).
[12] CAMFR is freely available from http://camfr.sourceforge.net.
[13] X. Jiang and C.M. Soukoulis, Phys. Rev. Lett. **85**, 70 (2000).
[14] K.S. Kunz and R.J. Luebbers, *The Finite Difference Time Domain Method for Electromagnetics* (CRC Press LLC, Boca Raton, FL, 1993).
[15] S. O'Brien and J.B. Pendry, J. Phys.: Condens. Matter **14**, 4035 (2002).
[16] R.W. Alexander, G.S. Kovener, and R.J. Bell, Phys. Rev. Lett. **32**, 154 (1974).
[17] A.M. Steinberg, P.G. Kwiat, and R.Y. Chiao, Phys. Rev. Lett. **71**, 708 (1993).
[18] W.M. Robertson, G. Arjavalingam, R.D. Meade, K.D. Brommer, A.M. Rappe, and J.D. Joannopoulos, Phys. Rev. Lett. **68**, 2023 (1992).